Iranian (Iranica) Journal of Energy & Environment
Journal Homepage: www.ijee.net
IJEE an official peer review journal of Babol Noshirvani University of Technology, ISSN:2079-2115

Removal of Pb^{2+} Ions from Aqueous Solutions by Modified Magnetic Graphene Oxide: Adsorption Isotherms and Kinetics Studies

G. Ramezani[1]*, S. E. Moradi [2], M. Emadi[2]

[1] *Department of Chemical Engineering, Marvdasht Branch, Islamic Azad University, Marvdasht, Iran*
[2] *Department of Chemistry, Marvdasht Branch, Islamic Azad University, Marvdasht, Iran*

P A P E R I N F O

Paper history:
Received 25 October 2020
Accepted in revised form 24 November 2020

Keywords:
Graphene
Adsorption isotherm
Kinetics
Surface modification

A B S T R A C T

Graphene oxide based nano-composites have attracted huge attention for wastewater treatment specially removal of heavy metals. This paper reports adsorption of Pb^{2+} onto modified magnetic graphene oxide with chitosan and cysteine (GO/Fe_3O_4/Chi/Cys). To study the adsorbent morphology, Field Emission Scanning Electron Microscope (FE-SEM) and Fourier Transform Infrared Spectrometer (FTIR) were used in different stages of surface modification. In order to reveal the nature of sorption process, linear forms of different adsorption isotherms such as Langmuir, Freundlich, Tempkin, and Dubinin–Radushkevich were studied. Experimental data were fitted well by Langmuir model with a maximum monolayer coverage capacity (q_{max}) of 86.21mg/g. Prediction of q_{max} from Langmuir model was in good agreement with maximum empirical adsorption capacity (q_{exp}=85.4mg/g). Various types of kinetic models such as pseudo-first-order, pseudo-second-order, Elovich, and intra particle diffusion were investigated to determine characteristic parameters in the adsorption process. The kinetic studies showed that pseudo-second-order model represents the adsorption process better than others due to its high correlation coefficient (R^2=0.9996). Therefore, the adsorption process is chemisorption.

***doi**: 10.5829/ijee.2020.11.04.05*

INTRODUCTION

Discharge of heavy metals into water as industrial wastes produced by battery producers, chemical products producers (e.g. plastic, glass and ceramic), metallurgy plants, paint producers, farmers, mines and the like has become one of the most serious environmental problems. This issue risks the general health of human and natural ecosystem [1, 2]. For example lead cations (Pb^{2+}) in drinking water are responsible for serious health issues such as disrupting the functions of the digestive system, nervous system and reproductive system [3, 4].

A variety of techniques are practiced to eradicate this pollutant from water resources which include chemical precipitation, reverse osmosis, ion exchange, membrane processes, adsorption on activated carbon, etc [5, 6]. Use of adsorption process for the removal of heavy metals from aqueous media is considered superior to other conventional methods in terms of cost effectiveness, high efficiency and simple design [7-9]. The adsorption technique in wastewater treatment is defined as a surface phenomenon, in which metal cations in aqueous solutions get accumulated on the surface of the adsorbent [10]. As the efficiency of the adsorption process depends on the number of adsorption sites and available specific surface area (SSA), choosing appropriate type of adsorbents plays a significant role in the efficiency of the process [11, 12].

In recent years, several different kinds of adsorbents have been synthesized for the removal of heavy metals from polluted waters, such as carbon nanotubes, fiber composites, agricultural wastes, modified activated carbon, magnetic nanocarbon, etc. There are some drawbacks for most of these adsorbents including low adsorption capacity, agglomeration, oxidizing in contact with the atmosphere and producing secondary water pollution after adsorption process [13]. To overcome these problems preparation of composite with other materials (surface modification) and using magnetic separation technique (MST) can be solutions. During magnetic separation, suspended absorbent is separated easily from aqueous solution due to the magnetic properties of Fe_3O_4 nanoparticles in absorbent's structure by applying an external magnetic field. Therefore, with this method, the possibility of secondary water pollution is significantly reduced [14, 15]. Also to

*Corresponding Author E-mail: ghazaaleh.ramezani@gmail.com (G. Ramezani)

Please cite this article as: G. Ramezani, S. E. Moradi, M. Emadi, 2020. Removal of Pb^{2+} Ions from Aqueous Solutions by Modified Magnetic Graphene Oxide: Adsorption Isotherms and Kinetics Studies, Iranian (Iranica) Journal of Energy and Environment, 11(4): 277-286.

improve the performance of adsorbents, the graphene-based materials such as graphene oxide (GO) and the reduced graphene oxide (RGO) sheets, which are basically forms of carbon, have been reported as promising candidates [16]. The excellent properties of GO such as high specific surface area and the presence of functional groups with oxygen (e.g. hydroxyl, epoxy, carboxyl, and carbonyl) in its structure have made it an effective material in the synthesis of different nano-composites [16-18]. These functional groups can play an important role in trapping metal cations. The adsorption efficiency of GO can be largely increased by modifying its surface with other materials that are included functional groups [19]. For this purpose, magnetic graphene oxide (GO/Fe_3O_4) was modified with chitosan (Chi) and cysteine (Cys) for adsorption of Pb^{2+} from water. Chi is a biocompatible polymer that provides high active sites due to amino ($-NH_2$) and hydroxyl (-OH) functional groups in its structure [20, 21]. Furthermore, Cys amino acid was used in the last step of surface modification due to its thoil (-SH) agent [22]. The chemical and physical properties of GO/Fe_3O_4/Chi/Cys were briefly characterized and the impact of effective variables on the adsorption performance such as contact time, pH solution, adsorbent dosage, and Pb^{2+} initial concentration were discussed in previous work. The results are represented in Table 1 [23].

The isotherms models are considered as equations that relate the adsorbate amount on the adsorbent with its concentration in solution containing heavy metal at a fixed temperature. They accurately describe the interaction between heavy metal cations and nano-composites. Therefore, there is a special need to study them in order to optimize the mechanisms of adsorption processes, express the surface properties and the adsorbents capacities [24, 25]. On the other hand, for engineering purposes like the design of industrial adsorption units, deep understanding of the adsorption process is necessary. Investigation of different adsorption kinetics models provides useful information to understand the dynamics of adsorption process [26].

The aim of this paper is to determine the most suitable isotherm and kinetic model for the adsorption of Pb^{2+}onto GO/Fe_3O_4/Chi/Cys through comparing the R^2s. At first, the morphology of surface and functional groups of GO/Fe_3O_4/Chi/Cys was investigated by using FE-SEM and FT-IR analysis. Next, linear forms of the Langmuir, Freundlich, Tempkin, and Dubinin–Radushkevich isotherms were utilized to determine the best-fit model. Finally, the results of several kinetic models (pseudo-first-order, pseudo-second-order, Elovich, and intra particle diffusion) were compared and studied.

TABLE 1. The optimal condition of Pb^{2+} adsorption onto GO/Fe_3O_4/Chi/Cys (at equilibrium concentration = 120 ppm)

$pH_{Optimum}$	5.75
$t_{Optimum}$	30 min
Adsorbent dosage	0.1 g
mg/gq_{exp}	85.4

MATERIALS AND METHODS

It should be noted that in the present study, modified Hummers method was used to synthesize GO and co-precipitation method was used to produce Fe_3O_4 nanoparticles. As covalent bonding of Cys to GO/Fe_3O_4 without an intermediate is complicated and inaccessible, in this study Chi was used as the middle layer. To bind Chi, simple technique of simultaneous precipitation was used and dilute base was added gradually to the mixture of Chi and GO/Fe_3O_4. This relatively simple method does not require complex laboratory equipment.

Materials

All the chemicals used in this study were of analytical grade. Chlorodic acid, Glacial Acetic acid, Pyridine 99%, $FeCl_2.4H_2O$, $FeCl_3.6H_2O$, sodium hydroxide (NaOH), L-cysteine, Natural Graphite powder and Ethanol absolute, were procured from Merck (Darmstadt, Germany). Sulfuric acid (H_2SO_4), acetic acid, sodium nitrate ($NaNO_3$), potassium permanganate ($KMNO_4$), hydrogen peroxide (H_2O_2), and glutaraldehyde (GA, 50% w/w solution in water) were bought from Sigma-Aldrich (Germany). Ammonia solution (25%) was supplied by Bismoot Company (Tehran, Iran). Powdery chitosan (CS, Mw 1.3x105 Da, 90% deacetylation) was obtained from Sinopharm Chemical Reagent Co., Ltd (Shanghai, China). All aqueous solutions were prepared with ultrapure water from Abanmpco Company, Mashhad, Iran. The stock solution of 1000 ppm Pb^{2+} was prepared by dissolving certain weight of dried $Pb(NO_3)_2$ obtained from Merck in ultrapure water. All the required concentrations of Pb^{2+} were obtained by diluting the stock solution, in 10 - 400 ppm range.

Instrumentation

The solution pH was measured using pH metrohm (Model 728) and adjusted using HNO_3 and KOH solutions (0.01 M). The metal concentration of samples was determined by linear calibration curves of atomic absorption spectrometer (PG instrument 990). After each test, all pipes and fittings were washed with ultrapure water and then were attached again to the system mechanically.

The chemical structure of GO/Fe_3O_4/Chi/Cys nanocomposite in each stage of surface modification was investigated using FTIR within the range of 500-4000cm^{-1}. The FTIR spectra were recorded with the

Spectrum Two FT-IR spectrometer from PerkinElmer company (U.K.). The morphology and textural structure of GO/Fe_3O_4/Chi/Cys were characterized by field emission scanning electron microscopy (FE-SEM, ZEISS SIGMA VP, Germany) with an accelerating voltage of 25 kV. Also, a 2 Tesla Neodymium Iron Boron (NdFeB) magnet was used to separate the nanoparticles from the solutions.

Preparation of adsorbent

In order to prepare GO/ Fe_3O_4/Chi/Cys following procedure was followed :

- As the first step, GO was prepared using modified Hummers method. Firstly, 5 g graphite powder and 5 g sodium nitrate were added to 150 ml sulfuric acid solution; the mixture was stirred at 0˚C. Then, 30g potassium permanganate was added to the mixture gradually. The mixed solution was diluted with ultrapure water until a bright brown color appeared. Next, 30 ml hydrogen peroxide solution (30% wt.) was added to the mixture. The mixture was centrifuged, washed several times with hydrogen chloride solution (10% v) and ultrapure water, and kept wet for the second step of surface modification.
- As the second step, 37.5 g $FeCl_3.6H_2O$ and 15 g $FeCl_2.4H_2O$ were dissolved in 100 ml hydrogen chloride solution (0.4 M) and added to 300 ml GO aqueous solution from the previous step. After adding Iron solution, the mixture was stirred for 2 h and added quickly to 700 ml ammonia solution (0.7 M). Ammonia solution was degasified earlier for 15 min with argon gas. The mixture was stirred at 60˚C for 2 h. Then, it was stirred at room temperature for 12 hours. The dark-black colored precipitate was collected and washed with ultrapure water until it reached neutral pH. Finally, the product of GO/ Fe_3O_4 was kept wet for the third step of surface modification.
- As the third step, 0.5 g Chitosan was dissolved in 30 ml acetic acid solution (4% v) and added to the GO/ Fe_3O_4 (from the previous step). Next, 0.5 ml glutardialdehyde (25% wt.) was added to the mixture and the mixture was mixed well for 10 min at room temperature. After that, the pH of mixture was adjusted to pH 10 using sodium hydroxide (2M). The resultant solution was refluxed at 60˚C for 1 h. Then, it was stirred at room temperature overnight. The mixture was centrifuged, washed with ultrapure water, and dried at 60˚C for 48 h. Finally, the product of GO/ Fe_3O_4 /Chi was crushed using ceramic mill.
- As the fourth and last step of surface modification, 0.5 ml glutaraldehyde (25% wt.) and 1 ml glacial acetic acid were suspended in pure ethanol (30 ml). The mixture was heated at 80˚C and stirred for 20 min. After that, 0.25 g L-cystein was added to 10 ml pure ethanol and heated at 120˚C.

Next, the two solutions were mixed together well and kept at 120°C for 24 h under reflux condition in an oil bath. The dark- green colored precipitate was centrifuged and washed with hot ethanol and ultrapure water. Finally, the product of GO/ Fe_3O_4/Chi/Cys was dried in an oven at 30˚C and crushed with ceramic mill.

Preparation of lead solutions

For preparing the stock solution (1000 ppm) of Pb^{2+} ions, 1.59 g $Pb(NO_3)_2$ was dissolved in ultrapure water and transferred into 1 liter volumetric flasks. This stock solution was diluted with ultrapure water to obtain a specific certain concentration range of Pb^{2+}standard solutions.

Adsorption isotherm experiment

In order to determine the GO/Fe_3O_4/Chi/Cys-Pb^{2+}adsorption isotherms, 0.1g of GO/Fe_3O_4/Chi/Cys was added to 40 ml Pb^{2+} solution at different initial concentrations of Pb^{2+}(from 120 to 400 ppm) at $pH_{Optimum}$ 5.75 and constant temperature of 295 K. The mixtures were put into a shaker with a constant shaking speed of 150 rpm. After optimum removal time ($t_{Optimum}$=30 min), the absorbent particles were separated quickly by applying an external magnetic field and the concentration of the remaining Pb^{2+} in the solutions was determined by linear calibration curves of atomic absorption spectrometer.

Adsorption kinetic experiment

In order to determine an optimum model for the kinetics, 40 ml Pb^{2+} solution was exposed to 0.1g GO/ Fe_3O_4/Chi/Cys for different time durations (ranging from 5 to 30min), at $pH_{Optimum}$ 5.75 and constant temperature of 295 K. After the adsorption process, the absorbent in samples was removed using the external magnetic field and the remaining concentration of Pb^{2+} was determined.

Data analysis

The adsorption capacity of GO/Fe_3O_4/Chi/Cys at the equilibrium (q_e in mg/g) was calculated based on the following equation:

$$q_e = ((C_0 - C_e)/m) \times v \quad (1)$$

Equation (2) represents the removal efficiency (%R) of Pb^{2+} by GO/Fe_3O_4/Chi/Cys:

$$\%R = ((C_0 - C_e)/C_0) \times 100 \quad (2)$$

In the both above equations, C_0 ($mg.L^{-1}$) and C_e ($mg.L^{-1}$) are the initial and equilibrium Pb^{2+} concentrations respectively, v (in liter) is the volume of the solution, and m(g) is the adsorbent mass [27, 28].

RESULTS AND DISCUSSION

Characterization of GO/Fe_3O_4/Chi/Cys

FE-SEM analysis

Morphological structure of synthesized adsorbent at the first and last stages of surface modification is shown in Figure 1. The purpose of this analysis is to observe structural changes in the surface of the synthesized adsorbent after the surface modification process. During the surface modification, the structure of GO changes clearly from porous and irregular shape (Figure 1a) to non-uniform, and heterogeneous shape (Figure 1b).

FT-IR analysis

The chemical structure of GO/Fe_3O_4/Chi/Cys nanocomposite in each stage was reported in Figures 2a - 2d.

The FTIR spectra of GO represented in (Figure 2a) showed a band at 1616cm^{-1} attributed to the υ(C=O) of the carboxy group. The absorption bands at 1384 and 1121$cm^{-1}$are both attributed to υ(C-O) mode. Another band is observed at 3411cm^{-1}that can be assigned to the υ(OH) vibration. This absorption band is wider in the IR spectra of GO/Fe_3O_4 (Figure 2b), which may be due to υ(OH) groups from Fe_3O_4 particles. Moreover, the band observed at 624$cm^{-1}$is attributed to the vibration of Fe–O stretching, which confirms that Fe_3O_4 particles have been bonded to GO nanosheets.

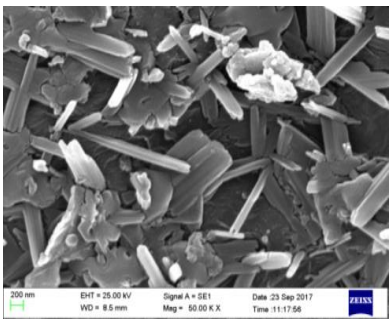

(a)

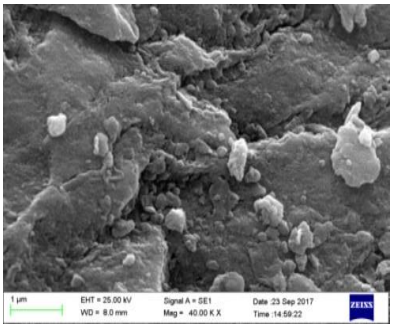

(b)

Figure 1. FE-SEM images of GO/ Fe_3O_4/Chi/Cys at first and last stages of surface modification, (a) FE-SEM micrograph of the synthesized GO, (b) FE-SEM micrograph of the synthesized GO/ Fe_3O_4/Chi/Cys adsorbent

The IR spectrum of GO/Fe_3O_4/Chi is shown in Figure 2c. This spectrum exhibited a strong absorption band at 3419cm^{-1} attributed to the υ(-NH). In addition, two obvious peaks at 3475 and 3548cm^{-1}can be attributed to the NH_2 vibrations. The absorption bands at 876cm^{-1}, 836cm^{-1}, and 777cm^{-1} are attributed to υ(N-H) vibrations. The free υ(OH^-) groups of chitosan can be observed at 3412cm^{-1}. The stretchings υ(S-H) (2079cm^{-1}) and υ(S-O) (1120cm^{-1}) can be observed in the FT-IR spectrum of GO/ Fe_3O_4/Chi/Cys (Figure 2d).

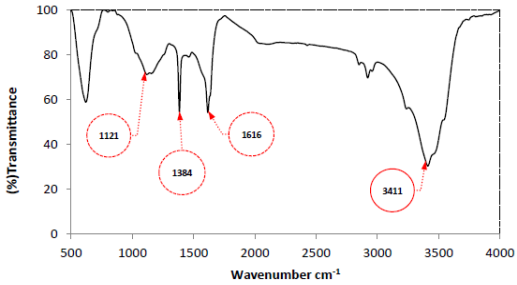

(a)

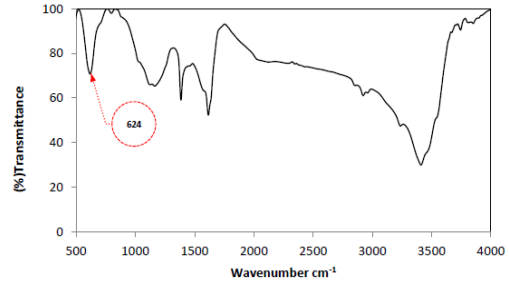

(b)

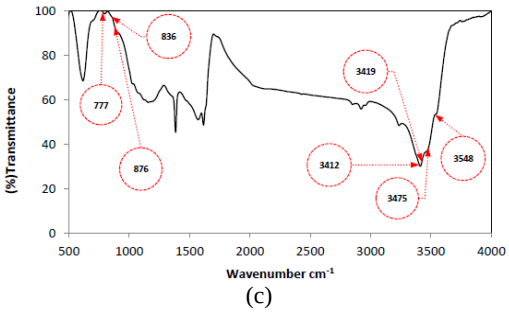

(c)

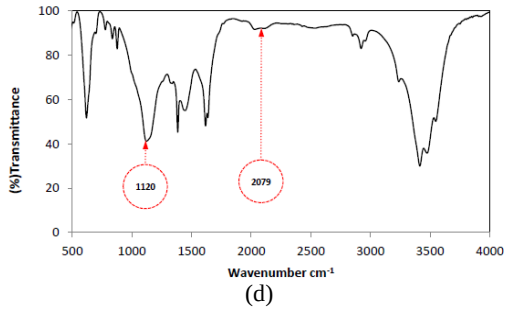

(d)

Figure 2. FT-IR spectra of GO/ Fe_3O_4/Chi/Cys at different stages of surface modification, (a) FT-IR spectra of the GO, (b) FT-IR spectra of the GO/ Fe_3O_4, (c) FT-IR spectra of the GO/ Fe_3O_4/Chi, d. FT-IR spectra of the GO/ Fe_3O_4/Chi/Cys

Equilibrium modeling

Study of adsorption isotherms

Adsorption isotherm is an informative diagram that demonstrates the relationship between adsorption volume of a chemical species by a solid phase in balance mode and fixed temperature. Adsorption isotherms are tools to describe and predict adsorption level, type, and severity of interaction between the adsorbent and adsorbate. In this research, the adsorption of Pb^{2+} ions onto GO/Fe_3O_4/Chi/Cys was studied at a temperature of 295K. Four different kinds of isotherms were used to fit equilibrium sorption data, including Langmuir, Freundlich, Tempkin, and Dubinin–Radushkevich Equation.

Langmuir isotherm model

There are four assumptions about Langmuir isotherm:

1. Uniform surface of the adsorbent; so that every adsorption site is the same as the others.
2. No interaction between the adsorbed molecules.
3. One mechanism controls all adsorptions.
4. Only one monolayer is created at the maximum adsorption: there is no deposit of adsorbate molecules on other, already adsorbed, molecules of adsorbate. Deposit happens only on the free surface of the adsorbent.

Nonlinear and Linear form of Langmuir isotherm are expressed as follows:

$$q_e = (q_{max} K_L C_e)/(1 + K_L C_e) \quad (3)$$

Linearizing Equation (3), we have:

$$(C_e/q_e) = (1/K_L . q_{max}) + (C_e/q_{max}) \quad (4)$$

where, C_e is the equilibrium concentration of adsorbate (mg/l) and q_e (mg/g) is the amount of adsorbed metal on the adsorbent at equilibrium. The q_{max} (mg/g) and K_L (the Langmuire constant) are computed from the slop and intercept of the graph C_e/q_e versus C_e, respectively [29].

In order to interpret the condition of the isotherm, separation factor or equilibrium parameter (R_L) is used. It is defined as follows [30]:

$$R_L = 1/(1 + K_L C_0) \quad (5)$$

where K_L is Langmuir constant related to the adsorption energy and C_0 is initial concentration. Different values of this dimensionless constant show that langmuir isotherm can be unfavorable $(R_L > 1)$, linear $(R_L = 1)$, favorable $(0 < R_L < 1)$, or irreversible $(R_L = 0)$.

Langmuir isotherm for Pb^{2+} ions adsorption onto GO/Fe_3O_4/Chi/Cys is depicted in Figure 3. The Langmuir constants were calculated and presented in Table 2.

Freundlich isotherm model

Freundlich model is a relationship that describes adsorption on a heterogeneous surface. Nonlinear form of Freundlich isotherm is expressed by the following equation:

$$q_e = k_f c_e^{(1/n)} \quad (6)$$

Freundlich adsorption parameters were determined by transforming the Freundlich Equation (6) into linear form.

$$\log q_e = \log K_F + (1/n) \log C_e \quad (7)$$

where $q_e (mg/g)$ is the amount of adsorbed metal on the adsorbent at equilibrium, C_e is the equilibrium concentration of adsorbate (mg/l), K_F is Freundlich isotherm constant (mg/g) related to the adsorption capacity, and n is adsorption intensity. The parameters k_f and n in this equation are determined from the intercept and slope of the plot of $\log q_e$ versus $\log C_e$ (Figure 4 and Table 2) [31].

Tempkin isotherm model

The Tempkin isotherm assumes that heat of adsorption (function of temperature) of all molecules in the layer would decrease linearly rather than logarithmic with coverage. The nonlinear form of this isotherm can be given by the following expression:

$$q_e = (RT/b_T) \ln a_T C_e \quad (8)$$

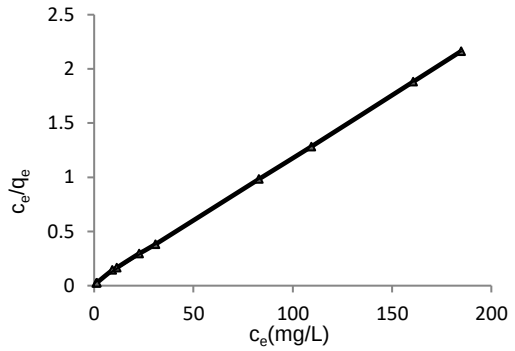

Figure 3. Langmuir adsorption isotherm of Pb^{2+} by GO/ Fe_3O_4/Chi/Cys (Experimental conditions employed: pH 5.75, agitation speed 150 rpm, adsorbent dosage 2.5 g/L)

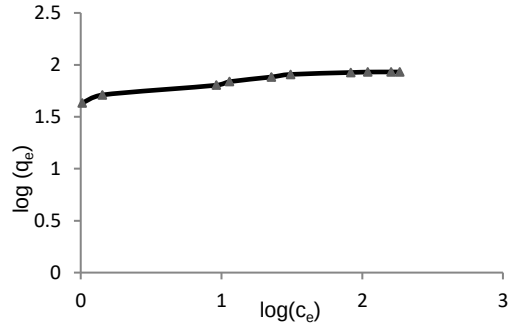

Figure 4. Freundlich adsorption isotherm of Pb^{2+} by GO/ Fe_3O_4/Chi/Cys (Experimental conditions employed: pH 5.75, agitation speed 150 rpm, adsorbent dosage 2.5 g/L)

TABLE 2. Model parameters obtained from linear fitting the experimental equilibrium data with the isotherm models (adsorbent dosage 2.5 g/L, pH 5.75, contact time 30 min)

	q_{max}(mg/g)	86.21
Langmuir	K_L(l/mg)	0.4659
	R^2	0.99
	$\frac{1}{n}$	0.125
Freundlich	n	7.97
	$K_F(mg/g)$	47.94
	R^2	0.92
	$b_T(kJ/mol)$	302.33
Tempkin	$a_T(L/g)$	340.3
	R^2	0.95
	$B(mol^2/J^2)$	2x10^{-7}
	$q_D(mg/g)$	78.57
Dubinin-Radushkevich	E (kJ/mol)	1.58
	R^2	0.84

Linearizing Equation (8), we have:

$$q_e = (RT/b_T)Lna_T + (RT/b_T)LnC_e \quad (9)$$

where $q_e(mg/g)$ is the amount adsorbed at equilibrium; R is universal gas constant (8.314 J/mol.K); T is Temperature in Kelvin and C_e is the equilibrium concentration of adsorbate(mg/l). The parameters of a_T (Temkin isotherm equilibrium binding constant (l/g)) and b_T(Temkin isotherm constant) are determined from the intercept and slope of the plot q_e versus LnC_e (Figure 5 and Table 2) [32].

Dubinin–Radushkevich isotherm model

Dubinin–Radushkevich isotherm is generally applied to express the adsorption mechanism with a Gaussian energy distribution onto a heterogeneous surface. The model has often successfully fitted high solute activities and the intermediate range of concentrations data well. The nonlinear and linear forms of the Dubinin–Radushkevich are represented in the following Equations (10) and (11), respectively:

$$q_D = q_D exp(-B\varepsilon^2) \quad (10)$$

$$Lnq_e = lnq_D - B\varepsilon^2 \quad (11)$$

where $q_e(mg/g)$ is the amount adsorbed at equilibrium, q_D is the theoretical saturation capacity ($mg.g^{-1}$), B is a constant related to mean free energy of adsorption per mole of the adsorbate (mol^2/J^2), and ε is the Polanyi potential and can be represented as:

$$\varepsilon = RTLn(1 + (1/C_e)) \quad (12)$$

where R is the universal gas constant ($8.314\ J/mol.k^{-1}$), T is the temperature (in Kelvin), and E is the mean

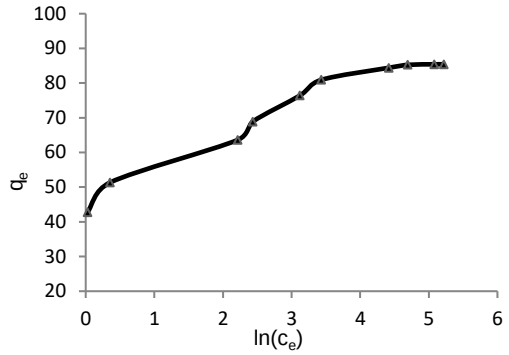

Figure 5. Tempkin adsorption isotherm of Pb^{2+} by GO/ Fe_3O_4/Chi/Cys (Experimental conditions employed: pH 5.75, agitation speed 150 rpm, adsorbent dosage 2.5 g/L)

sorption energy (kJ/mol) that is obtained as follows:

$$E = 1/(2B)^{0.5} \quad (13)$$

Equation (10) is linearized to Equation (11), which is used in Dubinin–Radushkevich graph (Lnq_e vs ε^2). Where B and q_D were determined from the slope and the intercept of the Dubinin–Radushkevich graph respectively (Figure 6 and Table 2) [33].

Langmuir, Freundlich, Tempkin, and Dubinin-Radushkevich models were used to determine the adsorption equilibrium between GO/Fe_3O_4/Chi/Cys and Pb^{2+} ions. The isotherm constants for the four models were obtained by linear regression method (Table 2) and R^2 were compared. Higher R^2 for an isotherm model indicates a better match between the experimental data and the isotherm model. From the data in Table 2, it can be concluded that Langmuir isotherm (R^2 were above 0.999) has a good agreement with experimental data and this isotherm is more suitable to predict the adsorption behavior. Moreover, q_{max} of Langmuir model was obtained equal to 86.206 mg/g, which is close to the q_{exp} (85.4mg/g). Hence, based on assumptions of Langmuir, the adsorption of Pb^{2+} ions

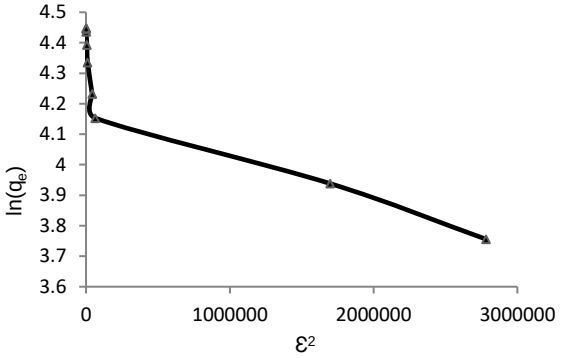

Figure 6. Dubinin-Radushkevich adsorption isotherm of Pb^{2+} by GO/ Fe_3O_4/Chi/Cys (Experimental conditions employed: pH 5.75, agitation speed 150 rpm, adsorbent dosage 2.5 g/L)

onto GO/Fe_3O_4/Chi/CS may be monolayer, homogeneous, and uniform. The values of R_L (between zero and 1) indicate a favorable adsorption.

Study of adsorption kinetic

One of the key issues about surface adsorption process is to examine the contact time that determines the pace of surface adsorption reaction. The pace is a key and important factor in the design of discrete industrial systems so that by determining the balance time, the adsorption time in the treatment facilities is determined [34].

In this research, four kinetic models were used to fit experimental data, pseudo-first-order, pseudo-second-order, Elovich, and intra particle diffusion equation.

Pseudo-first-order model

Nonlinear and linear forms of pseudo-first-order are expressed by the following equations respectively:

$$q_t = q_e[1 - \exp(-k_1 t)] \quad (14)$$

$$\log(q_e - q_t) = \log(q_{e1}) - (K_1/2.303)t \quad (15)$$

where q_e denotes the amount adsorbed at equilibrium in (mg/g), q_t in (mg/g) is the amount adsorbed at time t (min), and K_1 (min^{-1}) is the rate constant of pseudo-first-order model. The values of q_{e1} and K_1 were determined from the intercept and the slope of the graph of $\log(q_e - q_t)$ versus t (Figure 7 and Table 3) [35].

Pseudo-second-order model

The Pseudo-second-order equation is widely used for the adsorption of heavy metals from aqueous solutions. The pseudo-second-order equation can be written as:

$$q_t = (K_2 q_e^2 t)/(1 + q_e K_2 t) \quad (16)$$

Linearizing Equation (16), we have:

$$(t/q_t) = (1/K_2 q_e^2) + (1/q_{e2})t \quad (17)$$

where, q_e and q_t in (mg/g) are the adsorption capacities at equilibrium and at time $t(min)$ respectively, $K_2$is the corresponding kinetic constant $(g(mg^{-1}min^{-1}))$. Pseudo-second order kinetics plot is shown in Figure 8. The pseudo-second order kinetics parameters (q_{e2} and K_2) were determined respectively from the slope and the intercept of the graph t/q_t versus t (Table 3) [36].

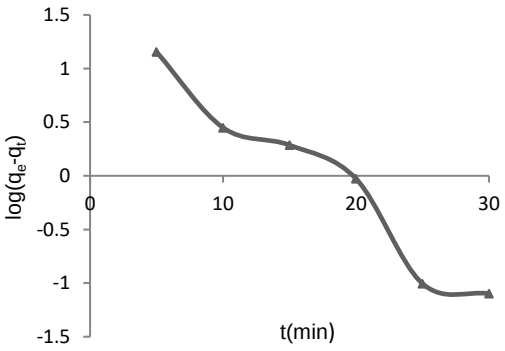

Figure 7. Pseudo first-order plot for the adsorption of Pb^{2+} on GO/ Fe_3O_4/Chi/Cys (Conditions: 0.1g adsorbent dosage, 150 rpm, and temperature 295 K

Elovich model

The Elovich equation was initially developed for studying the adsorption of gas-solid systems. In recent years, Elovich's equation has been applied to describe adsorption of inorganic substances on heterogeneous solid surfaces, mainly for heavy metal ions from aqueous solutions on biomass materials [37]. Nonlinear form of the Elovich model is generally expressed as follows:

$$(dq_t/dt) = \alpha e^{-\beta q_t} \quad (18)$$

Integrating Equation (18) for the boundary conditions (q_t=0 at t=0 and q_t=q_t at t=t), gives:

$$q_t = (1/\beta)\ln(\alpha\beta) + (1/\beta)\ln(t) \quad (19)$$

where α $(mg.g^{-1}min^{-1})$ is the initial adsorption rate and β is related to the extent of surface coverage and the activation energy for chemisorptions (mg/g) [38].

A linear plot obtained for Elovich model is shown in Figure 9. The plot of the q_t as a function of ln t provides β and α values. The results of Elovich kinetics are given in Table 3.

Intra particle diffusion model

The fourth synthetic model is called intra particle diffusion model. This model is used to describe multi-stage and competitive adsorptions. Multi-stage adsorption is featured with the transfer of molecules of the solved material from the solved phase to adsorbent particles surface and then transfer of these molecules into

TABLE 3. Calculated parameters of kinetic models for the adsorption of Pb^{2+} on GO/Fe_3O_4/Chi/Cys (adsorbent dosage 0.1g, 150 rpm, and temperature 295 K)

Pseudo-first-order model	$q_{e1}(mg/g)$	35.85
	$K_1(1/min)$	0.2098
	R^2	0.9492
Pseudo-second-order model	$q_{e2}(mg/g)$	84.03
	$K_2(g(mg^{-1}min^{-1}))$	0.0117
	R^2	0.9996
Elovich model	$\alpha\ (mg.g^{-1}min^{-1})$	16095.1
	$\beta(mg/g)$	0.1337
	R^2	0.824
Intra particle diffusion model	$k_{id}\ (mg.g^{-1}.min)$	3.8598
	c	62.06
	R^2	0.722

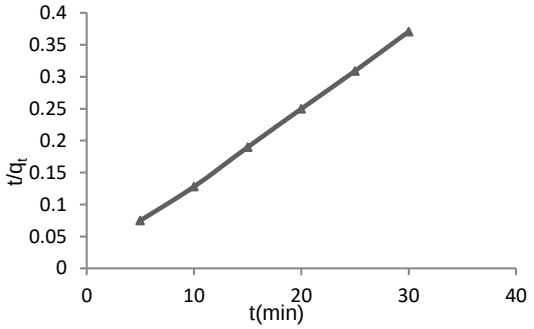

Figure 8. Pseudo second -order plot for the adsorption of Pb^{2+} on GO/ Fe_3O_4/Chi/Cys (Conditions: 0.1g adsorbent dosage, 150 rpm, and temperature 295 K

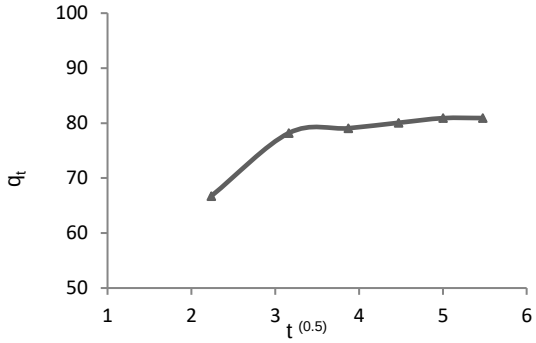

Figure 10. Intra particle diffusion plot for the adsorption of Pb^{2+} on GO/ Fe_3O_4/Chi/Cys (Conditions: 0.1g adsorbent dosage, 150 rpm, and temperature 295 K

solid surface pores. According to Weber and Moris, the volume of adsorption in the majority of adsorption processes is relative to $t^{0.5}$ rather than (t).

The Intra particle diffusion model equation is given by Equation (20):

$$q_t = k_{id} t^{0.5} + c \quad (20)$$

where $k_{id}(mg.g^{-1}.min)$ represents the intra-particle diffusion rate constant, $c\ (mg/g)$is a constant related to the thickness of the boundary layer, and t is time in min. The constants k_{id} and c can be determined from the slope and intercept of the linear plot q_t versus $t^{0.5}$(Figure 10 and Table 3).

The highest value of R^2 (close to 1) indicates the best kinetic model for describing adsorption of Pb^{2+} on GO/Fe_3O_4/Chi/Cys. It is clear from R^2 in Table 3 that pseudo-second-order model has higher R^2 value than other kinetic models. Moreover, the closeness of the adsorption capacities at equilibrium in second-order kinetic model ($q_{e2} = 84.03\ mg/g$) to q_{exp} (85.4mg/g) shows that the experimental data were well described by the pseudo-second-order kinetic model. This indicates that the adsorption process is chemisorption controlled.

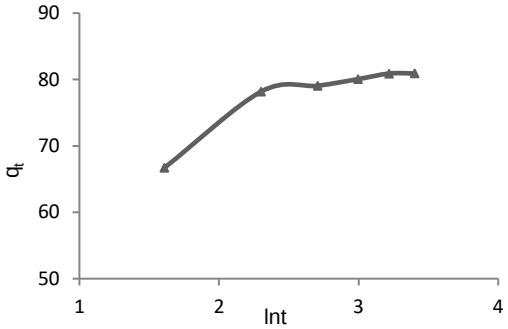

Figure 9. Elovich plot for the adsorption of Pb^{2+} on GO/ Fe_3O_4/Chi/Cys (Conditions: 0.1g adsorbent dosage, 150 rpm, and temperature 295 K

CONCLUSION

In this study, GO/Fe_3O_4/Chi/Cys nanocomposite was synthesized and used as adsorbent of Pb^{2+} ions from aqueous solution. The following results were obtained from the study.

1. The FT-IR analysis showed that all target functional groups such as epoxide, carbonyl, amino, and thiol were formed on the surface of the nancomposite and surface modification was successful in each stage.
2. The Isotherm studies showed that the Pb^{2+} adsorption process onto GO/Fe_3O_4/Chi/Cys followed the Langmuir isotherm model, which indicates that the adsorption process is monolayer, homogeneous, and uniform. The maximum Pb^{2+} adsorption capacity from Langmuir equation was obtained equal to 86.206 mg/g, which is close to q_{exp} (85.4mg/g).
3. Adsorption kinetic fitted well with pseudo-second-order model, which indicates that the adsorption process is chemisorption-controlled in nature.

Finally, this research work revealed that adsorption using magnetic composites such as GO/Fe_3O_4/Chi/Cys is becoming a promising option to replace commonly used adsorbents in removing Pb^{2+} ions from aquatic solutions, because the resulting product is able to decrease secondary water pollution significantly. Unique features of GO/Fe_3O_4/Chi/Cys like desirable adsorption capacity (85.4mg/g), homogeneous distribution of pores on the surface, biocompatibility, low-cost and ease of access make this material superior to other carbon-based composites for water purification.

ACKNOWLEDGMENT

The authors gratefully acknowledge the technical support for this work that was provided by Islamic Azad University of Marvdasht , Iran.

REFERENCE

1. Shan, R., Shi, Y., Gu, J., Wang, Y. & Yuan, H., 2020. Single and Competitive Adsorption Affinity of Heavy Metals toward Peanut Shell-Derived Biochar and Its Mechanisms in Aqueous Systems. Chinese Journal of Chemical Engineering, 28(5): 1375-1383. https://doi.org/10.1016/j.cjche.2020.02.012
2. Wang, J. & Chen, C., 2006. Biosorption of Heavy Metals by Saccharomyces Cerevisiae: A Review. Biotechnology advances, 24(5): 427-451. https://doi.org/10.1016/j.biotechadv.2006.03.001
3. Chen, C., Chen, Q., Kang, J., Shen, J., Wang, B., Guo, F. & Chen, Z., 2020. Hydrophilic Triazine-Based Dendron for Copper and Lead Adsorption in Aqueous Systems: Performance and Mechanism. Journal of Molecular Liquids, 298112031. https://doi.org/10.1016/j.molliq.2019.112031
4. Khazaei, M., Nasseri, S., Ganjali, M. R., Khoobi, M., Nabizadeh, R., Gholibegloo, E. & Nazmara, S., 2018. Selective Removal of Lead Ions from Aqueous Solutions Using 1, 8-Dihydroxyanthraquinone (Dhaq) Functionalized Graphene Oxide; Isotherm, Kinetic and Thermodynamic Studies. RSC advances, 8(11): 5685-5694. https://doi.org/10.1039/C7RA13603J
5. Davarnejad, R., Pishdad, R. & Sepahvand, S., 2018. Dye Adsorption on the Blends of Saffron Petals Powder with Activated Carbon: Response Surface Methodology. International Journal of Engineering, 31(12): 2001-2008. https://doi.org/10.5829/ije.2018.31.12c.02
6. Kumari, U., Siddiqi, H., Bal, M. & Meikap, B., 2020. Calcium and Zirconium Modified Acid Activated Alumina for Adsorptive Removal of Fluoride: Performance Evaluation, Kinetics, Isotherm, Characterization and Industrial Wastewater Treatment. Advanced Powder Technology, 31(5): 2045-2060. https://doi.org/10.1016/j.apt.2020.02.035
7. Biswas, S., Islam, M. M., Hasan, M., Rimu, S., Khan, M., Haque, P. & Rahman, M., 2018. Evaluation of Cr (Vi) Ion Removal from Aqueous Solution by Bio-Inspired Chitosan-Clay Composite: Kinetics and Isotherms. Iranian Journal of Chemical Engineering, 15(4): 63-80.
8. Chenab, K. K., Sohrabi, B., Jafari, A. & Ramakrishna, S., 2020. Water Treatment: Functional Nanomaterials and Applications from Adsorption to Photodegradation. Materials Today Chemistry, 16: 100262. https://doi.org/10.1016/j.mtchem.2020.100262
9. Dąbrowski, A., 2001. Adsorption—from Theory to Practice. Advances in colloid interface science, 93(1-3): 135-224. https://doi.org/10.1016/S0001-8686(00)00082-8
10. Zhang, X., Yan, L., Li, J. & Yu, H., 2020. Adsorption of Heavy Metals by L-Cysteine Intercalated Layered Double Hydroxide: Kinetic, Isothermal and Mechanistic Studies. Journal of Colloid and Interface Science, 562: 149-158. https://doi.org/10.1016/j.jcis.2019.12.028
11. Shafiee, M., Akbari, A. & Ghiassimehr, B., 2018. Removal of Pb (Ii) from Wastewater Using Henna; Optimization of Operational Conditions. Iranian Journal of Chemical Engineering, 15(4): 17-26.
12. Tohfegar, E., Moghaddas, J., Sharifzadeh, E. & Esmaeilzadeh-Dilmaghani, S., 2019. Synthesis and Characterization of Waterglass-Based Silica Aerogel under Heat Treatment for Adsorption of Nitrate from Water: Batch and Column Studies. Iranian Journal of Chemical Engineering, 16(4): 53-72.
13. Shojaei, Z., Iravani, E., Moosavian, M. & Torab, M. M., 2016. Removal of Cerium from Aqueous Solutions by Amino Phosphate Modified Nano Tio_2: Kinetic, and Equilibrium Studies. Iranian journal of chemical engineering, 13(2): 3-21.
14. El-Reash, A. & Gaber, Y., 2016. Magnetic Chitosan Modified with Cysteine-Glutaraldehyde as Adsorbent for Removal of Heavy Metals from Water. Journal of Environmental Chemical Engineering, 4(4): 3835-3847. https://doi.org/10.1016/j.jece.2016.08.014
15. Lashkenari, M., KhazaiePoul, A., Ghasemi, S. & Ghorbani, M., 2018. Adaptive Neuro-Fuzzy Inference System Prediction of Zn Metal Ions Adsorption by Γ-Fe2o3/Polyrhodanine Nanocomposite in a Fixed Bed Column. International Journal of Engineering, 31(10): 1617-1623. https://doi.org/10.5829/ije.2018.31.10a.02
16. Zhang, M., Cui, J., Lu, T., Tang, G., Wu, S., Ma, W. & Huang, C., 2020. Robust, Functionalized Reduced Graphene-Based Nanofibrous Membrane for Contaminated Water Purification. Chemical Engineering Journal, 404: 126347. https://doi.org/10.1016/j.cej.2020.126347
17. Shao, G., Lu, Y., Wu, F., Yang, C., Zeng, F. & Wu, Q., 2012. Graphene Oxide: The Mechanisms of Oxidation and Exfoliation. Journal of materials science, 47(10): 4400-4409. https://doi.org/10.1007/s10853-012-6294-5
18. Zhang, N., Qi, W., Huang, L., Jiang, E., Bao, J., Zhang, X., An, B. & He, G., 2019. Review on Structural Control and Modification of Graphene Oxide-Based Membranes in Water Treatment: From Separation Performance to Robust Operation. Chinese Journal of Chemical Engineering, 27(6): 1348-1360. https://doi.org/10.1016/j.cjche.2019.01.001
19. Oyedotun, K. O., Masikhwa, T. M., Lindberg, S., Matic, A., Johansson, P. & Manyala, N., 2019. Comparison of Ionic Liquid Electrolyte to Aqueous Electrolytes on Carbon Nanofibres Supercapacitor Electrode Derived from Oxygen-Functionalized Graphene. Chemical Engineering Journal, 375: 121906. https://doi.org/10.1016/j.cej.2019.121906
20. Qi, L. & Xu, Z., 2004. Lead Sorption from Aqueous Solutions on Chitosan Nanoparticles. Colloids and Surfaces A: Physicochemical Engineering Aspects, 251(1-3): 183-190. https://doi.org/10.1016/j.colsurfa.2004.10.010
21. Tripathi, S., Mehrotra, G. & Dutta, P., 2010. Preparation and Physicochemical Evaluation of Chitosan/Poly (Vinyl Alcohol)/Pectin Ternary Film for Food-Packaging Applications. Carbohydrate polymers, 79(3): 711-716. https://doi.org/10.1016/j.carbpol.2009.09.029
22. Depan, D., Girase, B., Shah, J. & Misra, R., 2011. Structure–Process–Property Relationship of the Polar Graphene Oxide-Mediated Cellular Response and Stimulated Growth of Osteoblasts on Hybrid Chitosan Network Structure Nanocomposite Scaffolds. Acta biomaterialia, 7(9): 3432-3445. https://doi.org/10.1016/j.actbio.2011.05.019
23. Ramezani, G. & Honarvar, B., 2019. Thermodynamic Study of (Pb^{2+}) Removal by Adsorption onto Modified Magnetic Graphene Oxide with Chitosan and Cysteine. Journal of Optoelectronical Nanostructures, 4(3): 73-94.
24. Al-Ghouti, M. A. & Da'ana, D. A., 2020. Guidelines for the Use and Interpretation of Adsorption Isotherm Models: A Review. Journal of Hazardous Materials, 393: 122383. https://doi.org/10.1016/j.jhazmat.2020.122383
25. Garba, Z. N., 2019. The Relevance of Isotherm and Kinetic Models to Chlorophenols Adsorption: A Review. Avicenna Journal of Environmental Health Engineering, 6(1): 55-65. https://doi.org/10.34172/ajehe.2019.08
26. Karimi, S., Yaraki, M. T. & Karri, R. R., 2019. A Comprehensive Review of the Adsorption Mechanisms and Factors Influencing the Adsorption Process from the Perspective of Bioethanol Dehydration. Renewable & Sustainable Energy Reviews, 107: 535-553. https://doi.org/10.1016/j.rser.2019.03.025
27. Amar, I. A., Sharif, A., Alkhayali, M., Jabji, M., Altohami, F. & AbdulQadir, M., 2018. Adsorptive Removal of Methylene Blue Dye from Aqueous Solutions Using Cofe1. 9mo0. 1o4 Magnetic Nanoparticles. Iranian (Iranica) Journal of Energy and Environment, 9(4): 247-254. https://doi.org/10.5829/ijee.2018.09.04.04

28. Khera, R. A., Iqbal, M., Jabeen, S., Abbas, M., Nazir, A., Nisar, J., Ghaffar, A., Shar, G. A. & Tahir, M. A., 2019. Adsorption Efficiency of Pitpapra Biomass under Single and Binary Metal Systems. Surfaces and Interfaces, 14: 138-145. https://doi.org/10.1016/j.surfin.2018.12.004
29. Raman, M. & Muthuraman, G., 2017. Removal of Binary Mixture of Textile Dyes on Prosopis Juliflora Pods–Equilibrium, Kinetics and Thermodynamics Studies. Iranian Journal of Energy & Environment, 8(1): 48-55. https://doi.org/10.5829/idosi.ijee.2017.08.01.09
30. Yu, F., Wu, Y., Ma, J. & Zhang, C., 2013. Adsorption of Lead on Multi-Walled Carbon Nanotubes with Different Outer Diameters and Oxygen Contents: Kinetics, Isotherms and Thermodynamics. Journal of Environmental Sciences, 25(1): 195-203. https://doi.org/10.1016/S1001-0742(12)60023-0
31. Matthews, T., Majoni, S., Nyoni, B., Naidoo, B. & Chiririwa, H., 2019. Adsorption of Lead and Copper by a Carbon Black and Sodium Bentonite Composite Material: Study on Adsorption Isotherms and Kinetics. Iranian Journal of Chemistry and Chemical Engineering, 38(1): 101-109.
32. Erhayem, M. E. & Masaaoud, M., 2019. Removal of Cadmium (Ii) from Aqueous Solutions onto Dodonaeae Viscose Leg Powder Using a Green Process: Isotherms, Kinetics and Thermodynamics. Iranian (Iranica) Journal of Energy & Environment, 10(1): 10-16. https://doi.org/10.5829/ijee.2019.10.01.02
33. Foo, K. Y. & Hameed, B. H., 2010. Insights into the Modeling of Adsorption Isotherm Systems. Chemical engineering journal, 156(1): 2-10. https://doi.org/10.1016/j.cej.2009.09.013
34. Azari, A., Salari, M., Dehghani, M. H., Alimohammadi, M., Ghaffari, H., Sharafi, K., Shariatifar, N. & Baziar, M., 2017. Efficiency of Magnitized Graphene Oxide Nanoparticles in Removal of 2, 4-Dichlorophenol from Aqueous Solution. Journal of Mazandaran University of Medical Sciences, 26(144): 265-281.
35. Ogbozige, F. & Toko, M., 2020. Adsorption Isotherms and Kinetics of Lead and Cadmium Ions: Comparative Studies Using Modified Melon (Citrullus Colocynthis) Husk. Iranian (Iranica) Journal of Energy & Environment, 11(2): 157-162. https://doi.org/10.5829/ijee.2020.11.02.10
36. Pandey, S., Singh, N., Shukla, S. & Tiwari, M., 2017. Removal of Lead and Copper from Textile Wastewater Using Egg Shells. Iranian (Iranica) Journal of Energy & Environment, 8(3): 202-209. https://doi.org/10.5829/ijee.2017.08.03.04
37. Fierro, V., Torné-Fernández, V., Montané, D. & Celzard, A., 2008. Adsorption of Phenol onto Activated Carbons Having Different Textural and Surface Properties. Microporous mesoporous materials, 111(1-3): 276-284. https://doi.org/10.1016/j.micromeso.2007.08.002
38. Cao, W., Dang, Z. & Lu, G.-N., 2013. Kinetics and Mechanism of Cr (Vi) Sorption from Aqueous Solution on a Modified Lignocellulosic Material. Environmental Engineering Science, 30(11): 672-680. https://doi.org/10.1089/ees.2012.0407

Persian Abstract

DOI: 10.5829/ijee.2020.11.04.05

چکیده

نانو کامپوزیت‌های مبتنی بر اکسید گرافن توجه زیادی را برای تصفیه فاضلاب به ویژه حذف فلزات سنگین جلب کرده‌اند. در این مقاله نتیجه ارزیابی جذب Pb^{2+} بر روی اکسید گرافن مغناطیسی اصلاح شده با کیتوزان و سیستئین ($GO/Fe_3O_4/Chi/Cys$) گزارش شده است. برای مطالعه مورفولوژی جاذب، میکروسکوپ الکترونی روبشی انتشار میدانی (FE-SEM) و طیف سنجی مادون قرمز تبدیل فوریه (FTIR) در مراحل مختلف اصلاح سطح استفاده شد. به منظور آشکار کردن ماهیت فرآیند جذب، به ترتیب فرم خطی ایزوترم‌های مختلف جذب مانند لانگمویر، فروندلیچ، تمپکین و دوبینین - رادوشکویچ مورد بررسی قرار گرفت. داده‌های آزمایشی با حداکثر ظرفیت پوشش تک لایه (q_{max}= 86.21mg/g) به خوبی توسط مدل لانگمویر برازش داده شد. پیش‌بینی q_{max} از مدل لانگمیر با حداکثر ظرفیت جذب تجربی (q_{exp}=85.4mg/g) مطابقت خوبی داشت. انواع مختلف مدل‌های سینیتیکی مانند شبه مرتبه اول، شبه مرتبه دوم، الوویچ و انتشار ذرات برای تعیین پارامترهای مشخصه در فرآیند جذب مورد بررسی قرار گرفت .مطالعات سینیتیکی نشان داد که مدل شبه مرتبه دوم به دلیل ضریب همبستگی بالاتر (R^2=0.9996)، فرآیند جذب را بهتر از سایرین نشان می‌دهد. بنابراین، فرآیند جذب شیمیایی است.